XI International Conference on Computational Plasticity. Fundamentals and Applications
COMPLAS XI
E. Oñate, D.R.J. Owen, D. Peric and B. Suárez (Eds)

PORE-SPACE CONTROLLED HARDENING MODEL IN PLASTICITY OF POROUS MATERIALS: APPLICATION TO THE ANALYSIS OF INDENTATION EXPERIMENTS

ROLAND TRAXL AND ROMAN LACKNER

Material Technology Innsbruck (MTI)
University of Innsbruck
Technikerstraße 13, A-6020 Innsbruck, Austria
e-mail: {Roland.Traxl, Roman.Lackner}@uibk.ac.at, www.uibk.ac.at/mti

Key words: Computational Plasticity, Indentation Analysis, Hardness, Porous Materials, Strength Homogenization

Abstract. Based on a multi-scale approach comprising a multi-scale material model and a respective finite-element (FE) analysis tool, the indentation response of porous materials is examined in this paper. The considered material is assumed to consist of a homogeneous Drucker-Prager-type matrix-phase and spherical pores. Non-linear homogenization is employed to derive both a strength criterion and a hardening rule at the macroscopic scale without the need of any additional non-physical material parameters. Hereby, the underlying macroscopic hardening is exclusively controlled by the evolution of the pore-space during loading. The material model is implemented in a FE program within the framework of elastoplasticity. The so-obtained analysis tool is applied to the analysis of indentation experiments commonly used for characterization and performance-based optimization of materials.

1 INTRODUCTION

Indentation experiments are commonly employed for determination of strength properties (hardness) of materials. Nowadays indentation analysis is applied on a great variety of materials and at various length scales, ranging from nanoindentation (e.g. Constantinides et al. [6]) to classical hardness measurements according to Tabor [15]. This gives scientists and engineers access to material properties even if ordinary test specimens for mechanical (compressive/tensile) testing are not available.

Meanwhile there are a number of publications treating indentation analysis for monolithic solids, focusing on the phenomenological aspect at the macro-scale (see e.g. Cheng et al. [5] for elastoplasticity, and Pichler et al. [14] for viscous material behaviour). In order to obtain a better understanding of indentation experiments, micro-mechanical changes

taking place in course of the indentation process are considered. E.g., application of limit analysis to porous material as presented in Cariou et al. [3] gives access to characteristic hardness-packing relations. Still, there are some underlying assumptions and restrictions: The change of material properties caused by the load history (hardening or softening) is neglected as well as piling-up or sinking-in effects. Besides, the so-obtained relations are only valid for virtually rigid materials and associated yielding.

Departing from the work presented in [3], a micromechanics-based material model based on nonlinear homogenization is developed and implemented in a FE program within the framework of non-associated hardening/softening elastoplasticity. Based on numerical simulations, the significance of the involved physical mechanism is investigated in regard to material characterization in indentation tests.

2 MATERIAL MODEL

The underlying material is assumed to consist of two phases: a solid phase and a pore phase. In the sequel, the existence of a representative elementary volume (REV) is assumed, which is equivalent with the requirement

$$d \ll L \ll h \ , \tag{1}$$

where d represents the characteristic size of pores, L the size of the REV, and h the indentation depth.

2.1 Elastic and plastic material properties

The pore phase of the considered two-phase material is characterized by its volume fraction φ and the shape of the pores. In the following, the pores are assumed to be spherical. The solid (matrix) phase is modeled as an elastoplastic material. Hereby, the domain of strength compatible stress states, E_M, is defined by a yield function according to the Drucker-Prager criterion, given by the cohesion c and the friction coefficient α of the material:

$$\boldsymbol{\sigma} \in E_M \ \Leftrightarrow \ f_M(\boldsymbol{\sigma}) = \sigma_d(\boldsymbol{\sigma}) + \alpha\sigma_m(\boldsymbol{\sigma}) - c \leq 0 \ , \tag{2}$$

where σ_m is the hydrostatic pressure, and σ_d the equivalent deviatoric stress:

$$\sigma_m = \frac{1}{3}\mathrm{tr}\boldsymbol{\sigma}, \quad \sigma_d = \sqrt{\frac{1}{2}\mathbf{s} : \mathbf{s}}, \quad \mathbf{s} = \boldsymbol{\sigma} - \mathbf{I}\sigma_m \ . \tag{3}$$

Within the elastic domain, the material is supposed to exhibit linear-elastic behavior, represented by the fourth-order tensor $\mathbb{C}_M$.

The domain E_M remains unchanged during loading (ideal plasticity). While an associated flow rule implies dilatation, a non-associated flow rule is adopted in order to describe volume-preserving yielding of the solid (matrix) phase, giving a plastic potential in the form:

$$g(\boldsymbol{\sigma}) = \sigma_d(\boldsymbol{\sigma}) \ . \tag{4}$$

2.2 Homogenization of elastic properties

Let V be the domain of the REV and V_M the domain of the solid (matrix) phase. In case of absence of pore pressure as supposed in the following, the homogenization problem of elastic properties is given in the framework of uniform strain boundary conditions by

$$\begin{aligned} \mathrm{div}\boldsymbol{\sigma} &= \mathbf{0} \qquad \text{in } V \\ \boldsymbol{\sigma} &= \mathbb{C}_M : \boldsymbol{\epsilon} \quad \text{in } V_M \\ \boldsymbol{\xi} &= \mathbf{E} \cdot \mathbf{x} \qquad \text{in } \partial V \end{aligned} \tag{5}$$

Therein, $\mathbf{x}$ is the position vector, $\mathbf{E}$ the macroscopic strain tensor, and $\boldsymbol{\xi}$ the displacement vector at the boundary of the REV. A macroscopic stress tensor $\boldsymbol{\Sigma}$ is defined as the average of the local stress $\boldsymbol{\sigma}$:

$$\boldsymbol{\Sigma} = \frac{1}{V}\int_V \boldsymbol{\sigma} dV = \langle \boldsymbol{\sigma} \rangle_V \ . \tag{6}$$

The homogenized stiffness tensor $\mathbb{C}_{hom}$ sought-after relates the macroscopic strain to the macroscopic stress:

$$\boldsymbol{\Sigma} = \mathbb{C}_{hom} : \mathbf{E} \tag{7}$$

For homogenization, the Mori-Tanaka scheme is applied, which yields the homogenized bulk and shear modulus as (see, for instance, [7] for details):

$$k_{hom} = \frac{4k_M\mu_M(1-\varphi)}{3k_M\varphi + 4\mu_M}, \quad \mu_{hom} = \mu_M \frac{(1-\varphi)(9k_M + 8\mu_M)}{9k_M(1+\frac{2}{3}\varphi) + 8\mu_M(1+\frac{3}{2}\varphi)} \tag{8}$$

Accordingly, the macroscopic stiffness tensor is obtained by:

$$\mathbb{C}_{hom} = 3k_{hom}\mathbb{J} + 2\mu_{hom}\mathbb{K}, \tag{9}$$

with

$$J_{ijkl} = \frac{1}{3}\delta_{ij}\delta_{kl}, \quad \mathbb{K} = \mathbb{I} - \mathbb{J} \ , \tag{10}$$

where δ is the Kronecker delta and $\mathbb{I}$ is the fourth-order unit tensor.

2.3 Homogenization of strength properties

While application of homogenization schemes to elastic properties is widely spread, most developments concerning non-linear behavior of composite material are relatively recent. An early and widely accepted criterion for porous Mises-type material was established by Gurson [8]. Since then, a number of contributions dealt with purely cohesive matrix phases, describing the material as fictitious non-linear elastic (see [16] for a survey). In [10], this approach was adopted for frictional solid phases with rigid inclusions

and in [7] for porous media, respectively. While these contributions derived the macroscopic yield criterion analytically, Pastor et al. [12] made use of simulation tools based on limit analysis.

An analytical formulation based on non-associated yielding was reported in [11]. Therein, the non-associated plasticity problem is interpreted as a nonlinear-viscoplastic problem with a pre-stress depending on the strain rate field $\dot{\boldsymbol{\epsilon}}$ to account for non-associated yielding. By introducing a representative strain rate (see [7]), this problem can be further simplified to a problem yielding an analogous structure as the problem of homogenization of elastic properties with pre-stress. Using the Mori-Tanaka scheme, the macroscopic yield function reads [11]:

$$F_{hom}(\boldsymbol{\Sigma}, \varphi) = \left(\frac{3}{4}\varphi - \alpha^2\right)\Sigma_m^2 + 2\alpha c(1-\varphi)\Sigma_m + \left(\frac{2}{3}\varphi + 1\right)\Sigma_d^2 - c^2(1-\varphi)^2 \ , \tag{11}$$

where φ represents the porosity of the material. For volume preserving yielding, the corresponding plastic potential is given by [11]:

$$G_{hom}(\boldsymbol{\Sigma}, \varphi) = \frac{3}{4}\varphi\Sigma_m^2 + \left(\frac{2}{3}\varphi + 1\right)\Sigma_d^2 \ . \tag{12}$$

In contrast to the model proposed in [11], φ is considered as hardening variable in this paper, depending on the volumetric change of the material. The total change of volume, ΔV, reads:

$$\Delta V = \Delta V_I + \Delta V_M \ . \tag{13}$$

ΔV_I and ΔV_M refer to the volume change in the inclusions (pores) and the matrix phase, respectively. ΔV_M, resulting only from elastic material response, is neglected (plastic deformation was assumed to be volume preserving). Thus, the macroscopic volumetric strain is given by:

$$E^{vol} = \frac{\Delta V}{V} \approx \frac{\Delta V_I}{V} = \frac{V_I + \Delta V_I}{V} - \frac{V_I}{V} = \varphi - \varphi_0 \ . \tag{14}$$

Since the initial φ_0 is a constant, expression (14) becomes in rate form:

$$\dot{\varphi} = \dot{E}^{vol} = \mathrm{tr}(\dot{\mathbf{E}}) \ . \tag{15}$$

2.4 Finite-element implementation

In the numerical simulation of indentation tests, geometric nonlinearities are taken into account. In large-strain elastoplasticity, a common concept is the multiplicative decomposition of the deformation gradient into an elastic and plastic part ($\mathbf{F} = \mathbf{F}^e\mathbf{F}^p$), as originally proposed in [9]. In case of isotropy, this is equivalent to the additive decomposition of the logarithmic strain measure (see, for instance, [13]). Thus, the measures used in the following refer to the logarithmic strain measure.

The material model is defined by

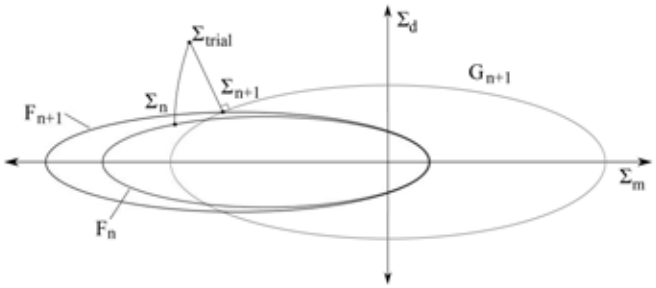

Figure 1: Illustration of the return mapping algorithm.

$$
\begin{aligned}
&\text{decomposition of strain:} && \mathbf{E} = \mathbf{E}^e + \mathbf{E}^p \\
&\text{elastic relation:} && \dot{\boldsymbol{\Sigma}} = \mathbb{C}_{hom} : \dot{\mathbf{E}}^e \\
&\text{flow rule:} && \dot{\mathbf{E}}^p = \dot{\gamma}\mathbf{r}(\boldsymbol{\Sigma}, \varphi) \\
&\text{hardening rule:} && \dot{\varphi} = \dot{\gamma} h(\boldsymbol{\Sigma}, \varphi) \\
&\text{Kuhn-Tucker condition:} && \dot{\gamma} F_{hom}(\boldsymbol{\Sigma}, \varphi) = 0 \ ,
\end{aligned}
$$

where

$$
\mathbf{r}(\boldsymbol{\Sigma}, \varphi) = \frac{\partial G_{hom}(\boldsymbol{\Sigma}, \varphi)}{\partial \boldsymbol{\Sigma}} \qquad \text{and} \qquad h(\boldsymbol{\Sigma}, \varphi) = \text{tr } \mathbf{r}(\boldsymbol{\Sigma}, \varphi) \ . \tag{16}
$$

Herein, $\dot{\gamma}$ denotes the plastic multiplier. For numerical implementation, these equations are discretized with respect to the time, reading for time increment $n+1$:

$$
\begin{aligned}
\boldsymbol{\Sigma}_{n+1} &= \mathbb{C}_{hom} : \mathbf{E}^e_{n+1} \\
\mathbf{E}^e_{n+1} &= \mathbf{E}^e_n + \Delta\mathbf{E}_{n+1} - \Delta\gamma\mathbf{r}(\boldsymbol{\Sigma}_{n+1}, \varphi_{n+1}) \\
\varphi_{n+1} &= \varphi_n + \Delta\gamma h(\boldsymbol{\Sigma}_{n+1}, \varphi_{n+1}) \\
\Delta\gamma F_{hom}(\boldsymbol{\Sigma}_{n+1}, \varphi_{n+1}) &= 0 \ .
\end{aligned} \tag{17}
$$

This non-linear system of equations is solved with a Newton scheme (return mapping) as illustrated in Figure 1. The trial stress is projected normally to the corresponding contour line of the plastic potential onto the updated yield surface. The incremental evolution of the yield surface is governed by the hydrostatic stress change within the correction step. If the hydrostatic stress of $\boldsymbol{\Sigma}_{trial}$ is smaller than that of $\boldsymbol{\Sigma}_{n+1}$ as in Figure 1, negative plastic volumetric strain and consequentially compaction occurs. The resulting decrease of porosity leads to an expansion of the yield surface (hardening).

3 INDENTATION ANALYSIS

3.1 Indentation

During indentation experiments, an indenter with a well-defined geometry is impressed into the surface of the material, while recording the applied force P and the penetration history. In general, the total deformation of the solid comprises a reversible and an

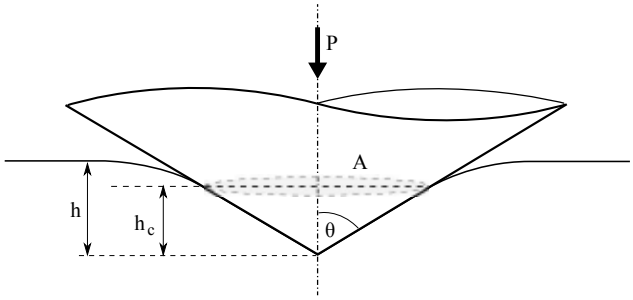

Figure 2: Conical indentation (h: indentation depth, h_c: penetration depth considering pile-up/sink-in, θ: half-angle of the cone, A: projected area of indent, P: applied force.

irreversible part. As a result, permanent deformation remains after unloading, giving access to the hardness of the material usually defined by the ratio of the applied force P and the projected area A of the residual imprint ($H = P/A$).

In this paper, the indentation of the three-sided pyramidal-shaped Berkovic indenter is treated. As this indenter belongs to the class of geometric self-similar indenter, it does not posses a characteristic length scale (unlike, e.g., the radius of spherical indenters). The geometry is completely described by the angle of inclination θ of the pyramid. Consequentially, the applied force P can be expressed in case of porous materials treated in the previous section as

$$P = f_P(E, \nu, c, \alpha, \varphi_0, d_i, h, \theta) \ . \tag{18}$$

Therein, the first four variables are the elastic and plastic properties of the matrix phase and φ_0 is the initial void ratio. The set of variables d_i represents the size of the pores. Applying the Π-theorem according to Cheng [4] yields:

$$\frac{P}{Eh^2} = \Pi_P \left(\frac{E}{c}, \nu, \alpha, \varphi_0, \frac{d_i}{h}, \theta \right) \ . \tag{19}$$

As the sizes of the pores are assumed to be very small in relation to the indentation depth (i.e., $d_i/h \to 0$), the function Π_P can be regarded as independent of the specific values of h and d_i. Thus, the resulting indentation problem is given by

$$\frac{P}{Eh^2} = \Pi_P \left(\frac{E}{c}, \nu, \alpha, \varphi_0, \theta \right) \ . \tag{20}$$

For describing the sink-in and pile-up effect, the variable h_c is introduced (see Figure 2). It defines the vertical distance between the tip of the indenter and the highest point of the material which is in contact with the indenter. Analogously to P, the following relations can be established:

$$h_c = f_h(E, \nu, c, \alpha, \varphi_0, d_i, h, \theta) \ , \tag{21}$$

which yields

$$\frac{h_c}{h} = \Pi_h \left(\frac{E}{c}, \nu, \alpha, \varphi_0, \theta \right) \ . \tag{22}$$

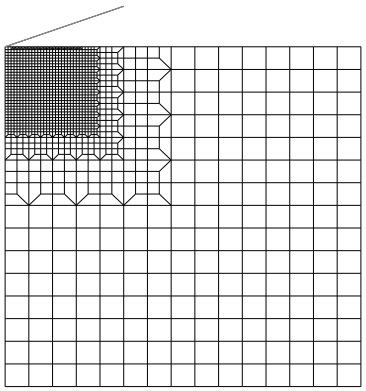

Figure 3: FE model.

3.2 Results

The indentation experiment was simulated with the FE program Abaqus using the user material subroutine and considering geometric nonlinearities. At large strain analysis, Abaqus delivers approximations of logarithmic strains to the user subroutine (c.f. [1]). Thus, the model given in Equation (17) can be employed without modifications.

Instead of using the real geometry of the Berkovic-Indenter, the indentation was simulated by means of a cone with an accordant A/h^2 ratio, giving a half-angle of the cone of 70.32°. Hence, the problem becomes axisymmetric and is modeled in two dimensions (see FE model in Figure 3). Through varying the parameters E/c, α, and φ_0, the yet unknown functions Π_P and Π_h are numerically evaluated.

Π_P and Π_h are evaluated for three different friction coefficients α (0.0, 0.25, and 0.5, see Figure 4). Note, that φ_0 denotes the initial porosity while the current porosity φ depends on the loading history and varies in space.

Low values for the E/c-ratios represent purely elastic material behavior while increasing E/c leads to an increasing influence induced by plasticity. In the elastic range, Π_h apparently does not depend on the porosity φ_0, while this influence increases for larger values for E/c. For materials with porosities larger than about 0.3, Π_h approaches 1.0 for large E/c-ratios. As expected, a higher friction coefficient α causes more stiffness (i.e., higher Π_P) in the elastoplastic domain.

Using Π_P and Π_h, the hardness of the material related to the cohesion is obtained by

$$\frac{H}{c} = \frac{E}{c} \frac{\Pi_P}{\Pi_h^2 \, \pi \, \tan^2\theta} \, . \tag{23}$$

In Figure 5, H/c is displayed and compared with results of Cariou et al.[3]. In [3], extensive parameter studies were performed, examining the material response for a number of different indenters and material properties. Therein, the material model is based on the same yield criterion as in the present work but restricted to associated yielding. As the analysis in [3] is based on limit analysis, neither the loading history and thus sink-in/pile-

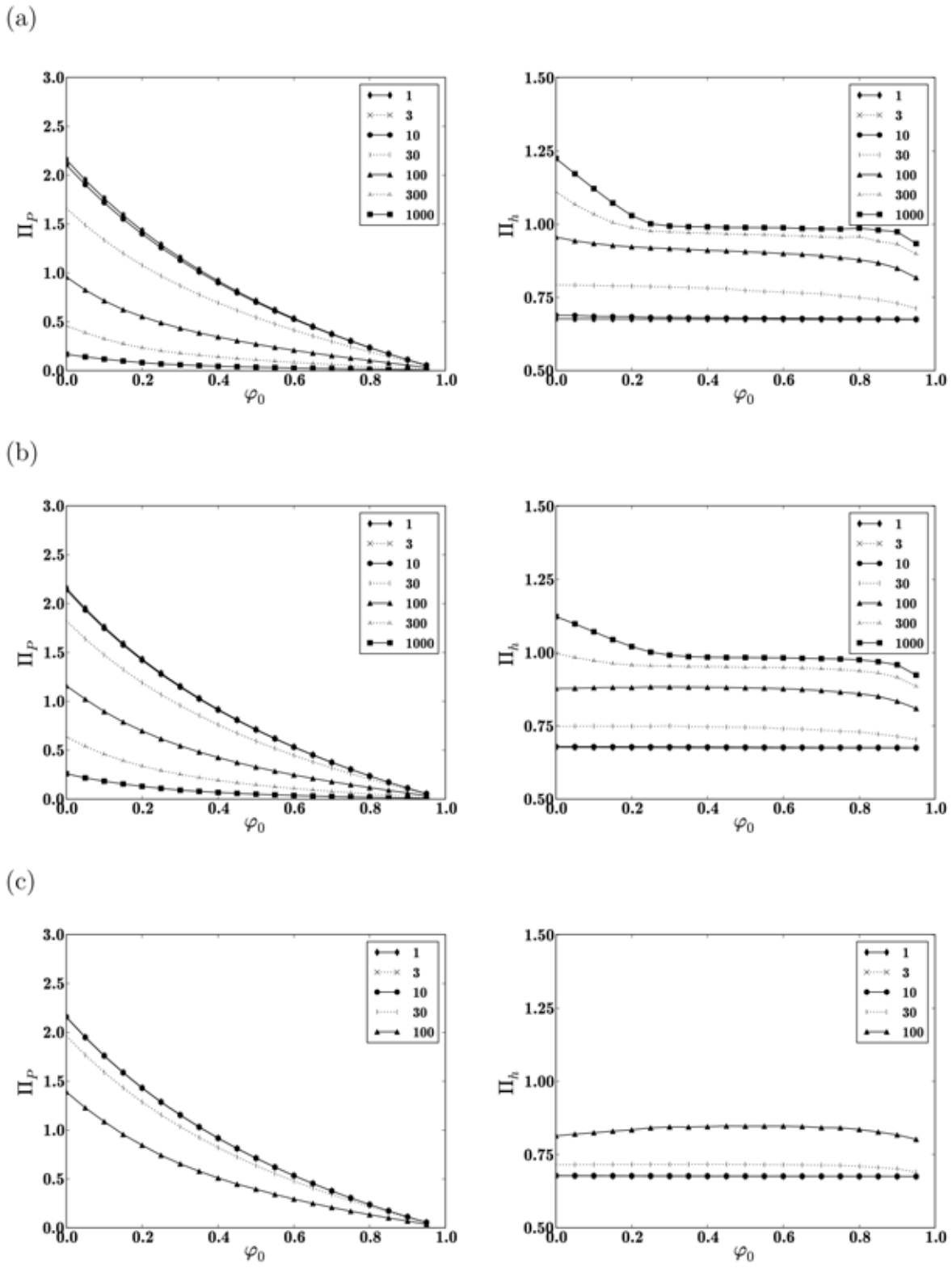

Figure 4: Functions Π_P and Π_h for different E/c-ratios: (a) $\alpha = 0$, (b) $\alpha = 0.25$, and (c) $\alpha = 0.50$.

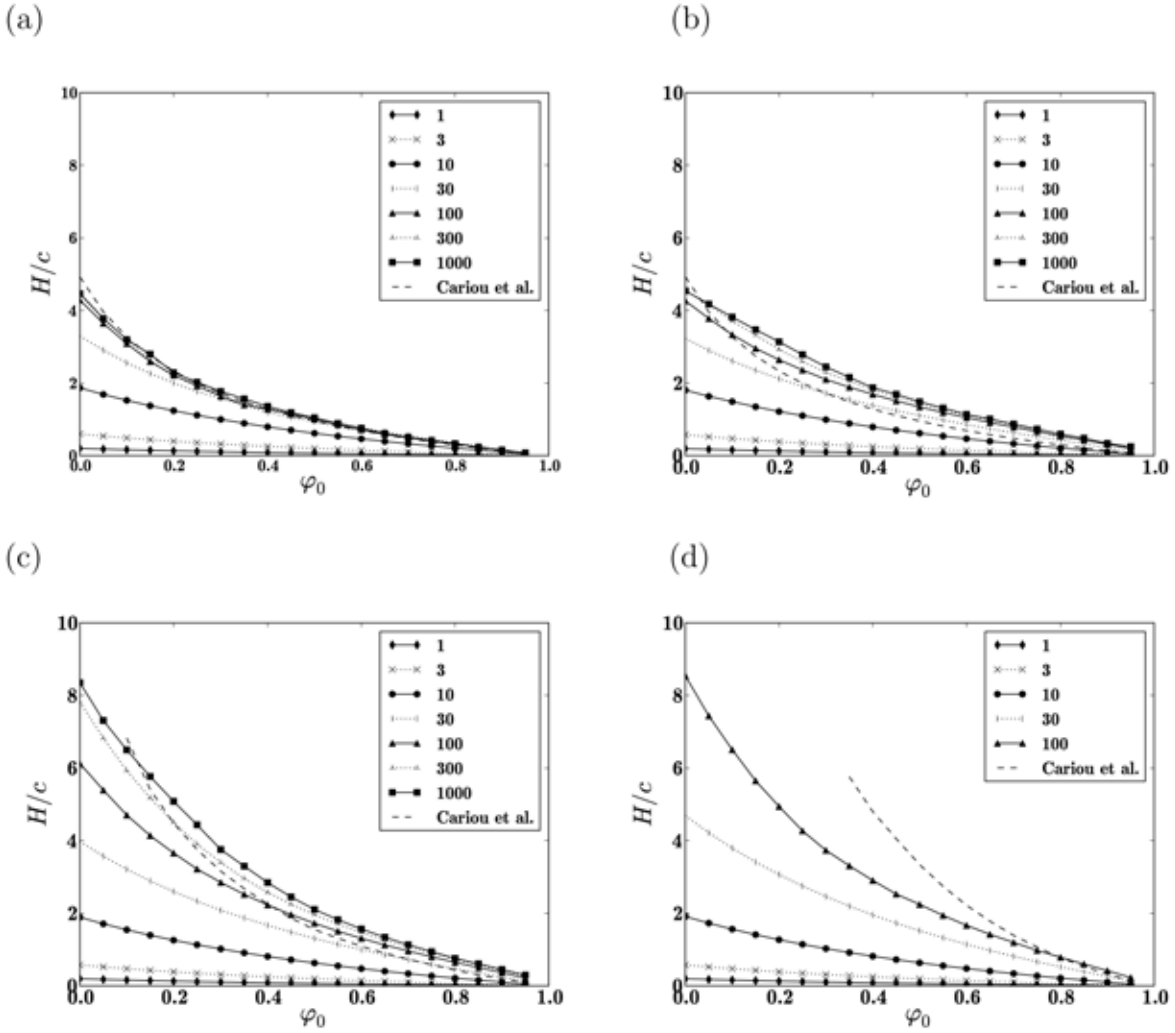

Figure 5: Related hardness H/c for different E/c-ratios: (a) $\alpha = 0$ without hardening, (b) $\alpha = 0$, (c) $\alpha = 0.25$, and (d) $\alpha = 0.50$.

up nor hardening effects were taken into account. Whereas a porosity range from $\varphi = 1.0$ to $\varphi_{crit} = 4/3\alpha^2$ was considered in [3] - for porosities below φ_{crit}, $F_{hom}(\boldsymbol{\Sigma}, \varphi)$ becomes a hyperbolic function - the porosity was varied between 0.0 and 1.0 in the present paper.

To highlight the possible influence of the loading history, Figure 5(a) shows simulation results where hardening, as proposed in this work, is neglected and associated yielding occurs. In this case, the plasticity model coincides with that in [3] while only the analysis methods differ. Since the reference solution from Cariou et al. [3] is valid for rigid materials, it represents an upper bound for the elastoplastic solutions. For large porosities, the solutions for different E/c are indeed bounded by this reference solution. For dense materials, the reference solution shows higher values for H/c which can be explained by the pile-up effect, which occurs at lower porosities and is neglected in Cariou et al. [3].

Figure 5(b) contains simulation results with pore-space controlled hardening, where

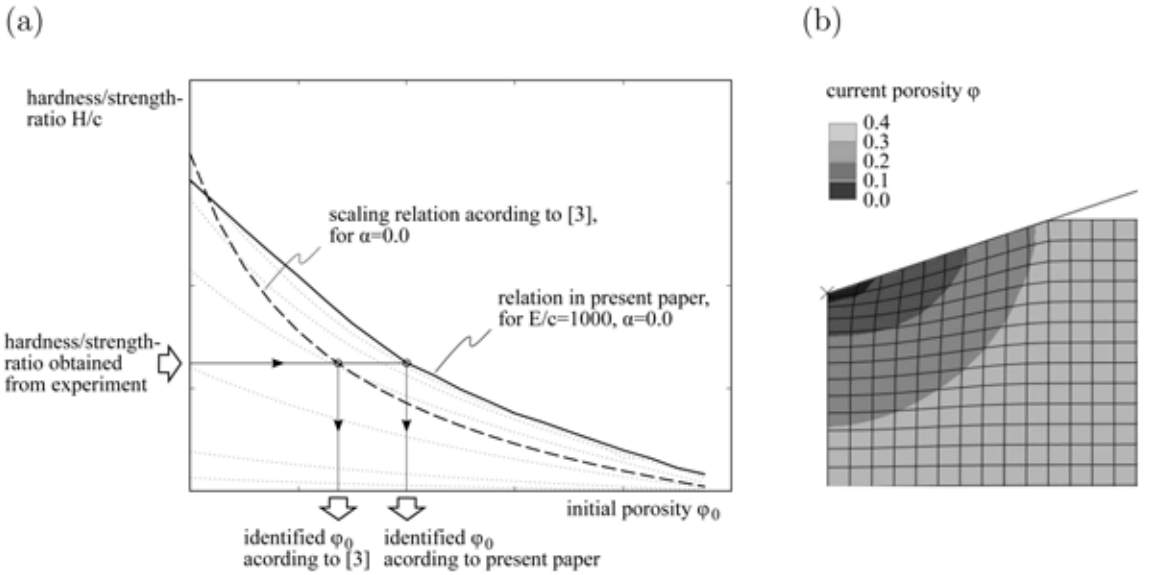

Figure 6: (a) Illustration of parameter identification where matrix material properties are known ($\alpha = 0.0$, $E/c = 1000$) and the initial porosity is looked after. (b) Contour plot of distribution of current porosity from FE analysis ($\varphi_0 = 0.4$, $\alpha = 0.0$, $E/c = 1000$).

the same material parameters were used as in Figure 5(a). Since no hardening occurs at absence of pore space, results for $\varphi = 0$ coincide in Figures 5(a) and (b). For $\varphi > 0$ however, an increase of the hardness as a consequence of hardening is clearly visible.

In case of $\alpha \neq 0$, the flow rule of the present material model becomes non-associated (see Equations (11) and (12)). While in [3] plastic dilation as well as plastic contraction are observed, only plastic contraction takes place in the present case since there are no distinct zones of hydrostatic tension. The absence of dilation reduces the hardness. A comparison of Figures 5(a) to (c) indicates, that the overall influence of the flow and hardening rule become larger for decreasing friction coefficients, providing improved estimates for the hardness when non-associated flow and hardening are taken into account.

4 CONCLUSION

Based on a continuum micro-mechanical approach described in Maghous et al. [11] a formulation of a material model was presented considering hardening controlled by change of porosity. By means of FE simulations, the indentation response of porous materials was evaluated for different materials, characterized by varying initial porosity, friction, and stiffness/strength-ratio. The so-obtained relations serve as a basis for identification of parameters of porous materials, giving insight into strength properties of material phase and/or into the composition of the material (porosity).

First results indicate that consideration of loading history and hardening may significantly improve the model performance, especially for high porosities and low friction angles, where the hardness may be clearly underestimated otherwise. For illustration

purpose, one application in parameter identification, shown in Figure 6(a), is considered where the properties of the matrix phase are known (E, ν, c, and α) and the initial porosity φ_0 should be determined. For an experimentally-determined hardness/strength-ratio H/c of 1.95, the scaling relation presented in this paper yields an initial porosity of $\varphi_0 \approx 0.4$ for $\alpha = 0$ and $\varphi_0 \approx 0.53$ for $\alpha = 0.25$, whereas the scaling relations in [3] underestimate the initial porosity with $\varphi_0 \approx 0.26$ and $\varphi_0 \approx 0.45$, respectively, representing somehow the spatial distribution of the porosity below the indenter tip (see Figure 6(b)) in an average manner.

ACKNOWLEDGMENT

The results reported in this paper were obtained within the research project "Model-based optimization of recycling building materials for the use as unbounded base-layer material", financially supported by the Austrian Research Promotion Agency (FFG). The authors gratefully acknowledge this support!

REFERENCES

[1] Abaqus Version 6.10 Documentation. Dassault Systèmes (2010).

[2] Barthélémy, J.F. and Dormieux, L. Détermination du critère de rupture macroscopique d'un milieu poreux par homogénéisation non linéaire. *Comptes Rendes Mecanique* (2003) **331**:271–276.

[3] Cariou, S., Ulm, F.J. and Dormieux, L. Hardness-packing density relation for cohesive-frictional porous materials. *Journal of the Mechanic and Physics of Solids* (2008) **56**:924–952.

[4] Cheng, Y.-T. and Cheng, C.-M. Scaling, dimensional analysis, and indentation measurements. *Material, Science and Engineering* (2004) **R44**:91–149.

[5] Cheng, Y.-T. and Cheng, C.-M. Scaling relationships in conical indentation of elastic - perfectly plastic solids. *Inernational Journal of Solids and Structures* (1999) **36**:1231–1243.

[6] Constantinides, G. , Ravi Chandran, K.S., Ulm F.-J. and Van Vliet K.J. Grid indentation analysis of composite microstructure and mechanics: Principles and validation. *Materials Science and Engineering A* (2006) **430**:189–202.

[7] Dormieux, L., Kondo, D. and Ulm, F.J. *Microporomechanics*. Wiley, Chichester, UK, (2006).

[8] Gurson, A.L. Continuum theory of ductile rupture by void nucleation and growth: part I - yield criteria and flow rules for porous ductile media. *ASME Journal of Engineering Materials and Technology* (1977) **99**:2–15.

[9] Lee, E.H. and Liu, D.T. Finite strain elastic-plastic theory with application to plane-wave analysis. *Journal of Applied Physics* (1967) **36**:1–6.

[10] Lemarchand, E., Ulm, F.J. and Dormieux, L. The effect of inclusions on the friction coefficient of highly-filled composite materials. *Journal of Engineering Mechanics* (2002) **128** (8):876–884.

[11] Maghous, S., Dormieux, L. and Barthélémy, J.F. Micromechanical approach to the strength properties of frictional geomaterials. *European Journal of Mechanics A/Solids* (2009) **28**:179–188.

[12] Pastor, J., Thoré, Ph. and Pastor, F. Limit analysis and numerical modeling of spherically porous solids with Coulomb and Drucker-Prager matrices. *Journal of Computational and Applied Mathematics* (2010) **234**:2162–2174.

[13] Perić, D., de Souza Neto, E.A. and Owen, D.R.J. *Computational Methodes for Plasticity* . John Wiley & Sons, Chichester, (2008).

[14] Pichler, C., Lackner, R. and Ulm, F.J. Scaling relations for viscoelasticcohesive conical indentation. *International Journal of Materials Research* (2008) **99**:836–846.

[15] Tabor, D. A simple theory of static and dynamic hardness. *Proceedings of the Royal Society, Series A* (1948) **192**:247–274.

[16] Zaoui, A., Continuum micromechanics: survey. *Journal of Engineering Mechanics* (2002) **128** (8):808–816.